Paul Condron, BSc (Hons)
Mātai Medical Research Institute
—
Gisborne, New Zealand

Mark Bydder, PhD
Mātai Medical Research Institute
—
Gisborne, New Zealand

Samantha J. Holdsworth, PhD
Mātai Medical Research Institute
—
Gisborne, New Zealand

Ultra-high contrast MR of the brain and spinal cord

By Paul Condron, BSc (Hons), MRI Charge Technologist, Mark Bydder, PhD, Senior Research Fellow, Samantha J. Holdsworth, PhD, Executive Director at Mātai Medical Research Institute and Associate Professor at the University of Auckland, Daniel M. Cornfeld, MD, FRANZCR, Clinical Lead, and Graeme M. Bydder, FRANZCR, Scientific Advisory Board Member, Mātai Medical Research Institute, Gisborne, New Zealand

Introduction

The ability to visualize differences in signal intensity, or contrast, between normal and abnormal soft tissue is the most important feature of MR in clinical diagnosis. Efforts to improve the MR visualization of lesion contrast have included modification of sequence parameters, use of higher field strengths and development of novel MR contrast agents.

At Mātai Medical Research Institute, researchers are developing a new approach to increasing contrast, namely ultra-high contrast (UHC)[‡], which radically improves visualization of soft tissue contrast. Here we explain the background and show images obtained with the new technique.

Background

UHC is a descriptive term applied to MR images that show abnormalities with very high contrast when conventional state-of-the-art MR images show little or no abnormality. The most common way of improving contrast in MR is to increase the static magnetic field. This increases the image SNR and can be used to improve soft tissue contrast, the speed of the examination and/or spatial resolution. However, UHC MR achieves its goal of radically increased contrast without increasing the static or gradient magnetic field. It uses readily available pulse sequences that exist on most machines and can be rapidly implemented on most existing MR systems at very little cost.

The approach is underpinned by a different way of understanding image contrast in MR. This employs tissue property filters (TP-filters),which provide a clear relationship between changes in tissue properties such as T1 and T2, and the contrast these changes produce on images, as explained in the next section.

UHC MR can have its primary basis in mathematical manipulation of the sequences used for acquisition and the resultant signals. It can also have its primary basis in the physics of MR such as the process of magnetization transfer (MT).

UHC MR images are easily recognized and, since the technique employs sequences commonly used in MR, UHC MR usually fits well with established imaging protocols.

UHC MR is targeted at applications where state-of-the-art MR does not usefully show abnormalities, and so it is usually obvious where it should be used. Thus, it is not a technique in search of an application. UHC MR is complementary to existing sequences which show contrast from larger changes in tissue properties in disease, while UHC shows contrast from smaller changes in tissue properties in disease.

In addition, evaluation of UHC MR is usually straightforward and normally involves direct comparison of conventional images with UHC images and correlation with clinical data (and pathology if available).

[‡] Technology in development that represents ongoing research and development efforts. These technologies are not products and may never become products. Not for sale. Not cleared or approved by the US FDA or any other global regulator for commercial availability.

Daniel M. Cornfeld, MD, FRANZCR
Mātai Medical Research Institute
—
Gisborne, New Zealand

Graeme M. Bydder, FRANZCR
Mātai Medical Research Institute
—
Gisborne, New Zealand

The next section describes tissue property filters and the following sections describe an example of UHC MR based on math. This is followed by an example of UHC MR based on physics (MT).

Tissue Property filters (TP-filters)

Instead of illustrating image contrast by plotting longitudinal and then transverse magnetization (M_z and then M_{xy}) against time using the Bloch equations as in Figure 1, it is possible to use plots of signals against T1 and T2 respectively. These plots are TP-filters.[1]

The T1-filter of the IR sequence is shown in phase-sensitive or signed form in Figure 2A where it is a monotonic low pass filter, and in magnitude form in Figure 2B where it is a negative unipolar filter. The maximum size of the slopes of these two filters are shown with red lines in Figures 2A and 2B.

When TI is increased, the magnitude IR T1-unipolar filter shifts to the right as shown in Figure 3. Figure 3A (left) shows the IR T1-filter with a short TI_s (e.g., the Short TI IR or STIR sequence) for brain where gray matter (G) has a higher signal than white matter (W). The slope of the T1-filter between W and G is moderately positive (red line).

When the TI is increased to an intermediate TI, TI_I, as in Figure 3B (center), the T1-filter is shifted to the right. W and G are fixed in the same position on the X axis, and W now has a higher signal than G. The slope of the T1-filter between W and G is strongly negative (red line).

When the TI is increased further to a long TI, TI_L, the T1-filter is displaced further to the right, as in Figure 3C (right) where W has a slightly higher signal than G, and the slope of the T1-filter between them is mildly negative (red line).

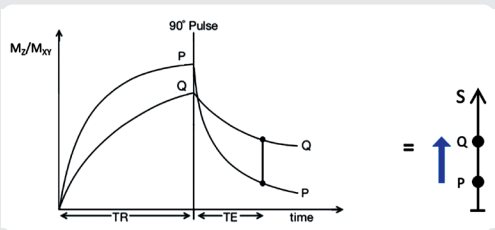

Figure 1. Plot of M_Z/M_{XY} against time for a T2-weighted version of the SE sequence for two tissues P (with a shorter T1 and T2) and Q (with a longer T1 and T2). Overall T1 and T2 dependent contrast between P and Q is shown with the positive blue arrow on the right.

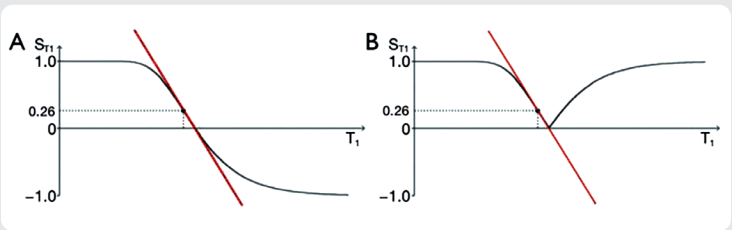

Figure 2. IR T1-filters with plots of signal S_{T1} against T1 in (A) phase-sensitive and (B) magnitude forms. (A) is a low pass filter and (B) is a negative unipolar filter. (A) shows both positive and negative values for S_{T1} whereas (B) shows negative values "reflected" across the X axis so they become positive. The maximum size of the slopes of the two T1-filters which are tangential to the slope are shown as red lines. The slopes are negative in both cases.

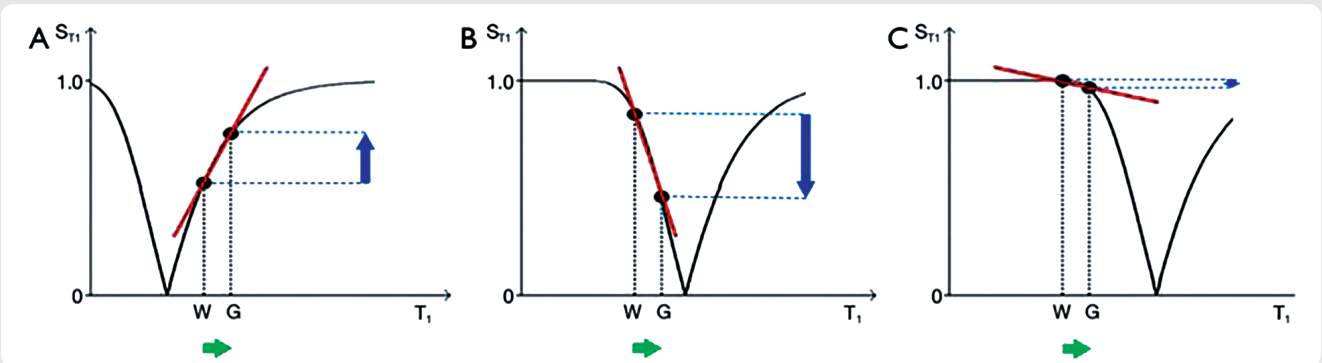

Figure 3. The long TR IR sequence. Negative T1-unipolar filters for (A, left) short TI_s, (B, center) intermediate TI_I and (C, right) long TI_L including white (W) and gray (G) matter. Signal S_{T1} is plotted against T1 in each case (black curves). The positions of W and G are the same at each of the three TIs. TI is increased from TI_s (left) to TI_I (center) and increased further to TI_L (right). In (A), (B) and (C), the increase in T1 from W to G (horizontal positive green arrows) is multiplied by the relevant slopes of the filters (red lines) to produce contrast. This is moderately positive, strongly negative, and mildly negative contrast in (A), (B) and (C) respectively (vertical blue arrows).

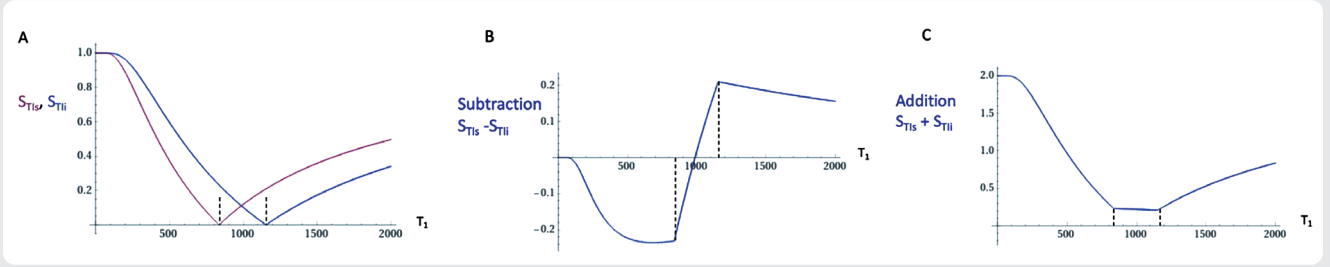

Figure 4. (A) Unipolar IR, (B) subtracted IR (SIR) and (C) Added IR (AIR) T1-filters. T1 is shown along the X axes in ms. (A) shows a TI_s T1-unipolar filter (pink) and a TI_i T1-unipolar filter (blue), (B) shows the subtraction (S_{TIs} - S_{TIi}) IR or SIR T1-bipolar filter, and (C) shows the addition (S_{TIs} + S_{TIi}) IR or AIR T1- filter. The vertical lines divide the X axes into lowest, middle and highest Domains (lD, mD and hD). The mD contains T1 values between the vertical dashed lines. In (B) the slope of the curve of the SIR T1-filter in the mD is about double that of the S_{TIs} T1-filter (pink in [A]). In (C) the signal at T1=0 is doubled to 2.0, and the signal in the mD is reduced to about 0.20 in the nearly linear, slightly downward sloping central part of the AIR T1-filter (i.e., in the mD).

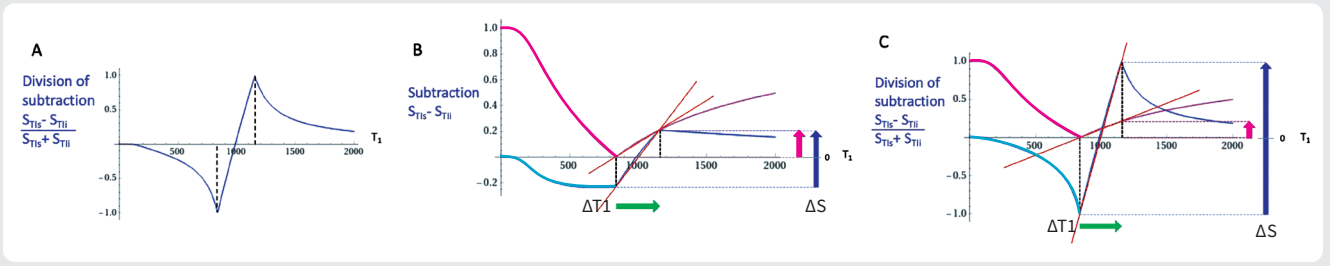

Figure 5. (A) Division of the SIR T1-bipolar filter in Figure 4B by the addition T1-filter AIR in Figure 4C to give the dSIR T1-bipolar filter. T1 is shown along the X axis in ms. (B) Comparison of the conventional IR S_{TIs} T1-unipolar filter (pink) with the SIR T1-bipolar filter (blue) for a small increase in T1 (horizontal positive green arrow, ΔT1). (C) Comparison of the S_{TIs} T1-unipolar filter (pink) with the dSIR T1-bipolar filter (blue) for the same small increase in T1. (B) The contrast produced by the SIR T1-bipolar filter is about twice that produced by the IR T1-unipolar filter (blue and pink arrows). (C) The contrast produced by the dSIR T1-bipolar filter is about 10 times greater than that produced by the IR T1-unipolar filter (blue and pink arrows). The display gray scale has no negative values so white matter appears on it as zero signal (black) at the lowest part of the display scale when using both the T1-filters shown in each of (B) and (C).

Using the small change approximation of differential calculus, the contrast (difference in signal) produced by each T1-filter from the difference in T1 from W to G (horizontal green arrows in Figures. 3A, 3B and 3C) is the size of this difference in T1 multiplied by the slopes of the respective T1-filters (i.e., by their first derivatives, the red lines). This contrast is shown by the vertical blue arrows in Figure 3 and is moderately positive in Figure 3A, highly negative in Figure 3B and mildly negative in Figure 3C. The slopes of the T1-filters (red lines) show the contributions the sequence makes to contrast in each case.

UHC MR using math: the divided Subtracted IR (dSIR) sequence[2-5]

Two conventional magnitude IR T1-unipolar filters with different TIs, namely TI_{SHORT} = TI_s and $TI_{INTERMEDIATE}$ = TI_i are shown in Figure 4A. The subtraction: first TI_s T1-filter minus the second TI_i T1-filter produces the subtracted IR (SIR) T1-bipolar filter shown in Figure 4B. The vertical dashed lines at the null points of the two IR T1-filters shown in Figure 4A divide the X axis in Figure 4B into the lowest Domain, the middle Domain (mD) and the highest Domain. In the mD in Figure 4B (between the two dashed lines) the size of the slope of the SIR T1-bipolar filter is about double that of the IR T1-filters shown in Figure 4A.

The two IR T1-filters shown in Figure 4A can also be added to give the Added IR (AIR) T1-filter shown in Figure 4C. In its mD, which is bounded by the vertical dashed lines, the signal is reduced to about 0.20 compared with its value of 2 at T1 = 0 (i.e., about one tenth). Figure 5A shows a divided SIR (dSIR) T1-bipolar filter in which the SIR T1-bipolar filter in Figure 4B is divided by the AIR T1-filter in Figure 4C, i.e., $\frac{\text{difference}}{\text{sum}}$.

The resulting dSIR T1-bipolar filter (Figure 5A) shows a negative pole and a positive pole. Its mD shows a highly positive nearly vertical slope, which is about 10 times larger than the slopes of the IR T1-filters shown in Figure 4A. The dSIR filter has maximum and minimum values of ±1.

Figure 5B compares the contrast produced by a conventional S_{TIs} IR T1-unipolar filter (pink) to that from the SIR T1-bipolar filter (blue) shown in Figure 4B from the same increase in T1 (horizontal positive green arrow, ΔT1). ΔT1 is multiplied by the slopes of the respective S_{TI} IR and SIR filters (red lines) to produce the differences in signal ΔS, i.e., the contrast from each of them. This is shown by the vertical pink and blue arrows on the right. The SIR T1-bipolar filter generates about twice the contrast (blue arrow) of the S_{TIs} IR T1-unipolar filter (pink arrow) from the same increase in T1, ΔT1.

Figure 5C compares the contrast produced by the S_{TIs} IR T1-unipolar filter (pink) to that produced by the dSIR T1-bipolar filter shown in Figure 5A (blue). The increase in T1 (horizontal positive green arrow, ΔT1) is multiplied by the slopes of the respective S_{TIs} IR

and dSIR filters (red lines) to produce the differences in signal ΔS, or contrast generated by the two filters. This is shown by the vertical pink and blue arrows on the right. For the same increase in T1 (ΔT1), the dSIR T1-bipolar filter produces about 10 times more contrast than the S_{TIs} IR T1-unipolar filter. The S_{TIs} IR T1-filter is that of a conventional TI IR sequence such as MP-RAGE (magnetization prepared-rapid acquisition gradient echo).

To produce the large increase in contrast shown in Figure 5C, the dSIR sequence is typically targeted at the small increase in the T1 of normal tissue produced by disease (shown by the horizontal green arrow), which is positioned within the steeply sloping mD of the dSIR T1-bipolar filter. This is done by choosing appropriate values of TI_s and TI_i. The target is often small increases in the T1 of white matter. High contrast can also be produced by difference or change in T1 within the lower part of the highest Domain and the upper part of the lowest Domain where the dSIR T1-bipolar filter has relatively steep slopes. More detail is available in reference.[3]

UHC MR — physics based[6]

With 2D multislice acquisitions, there may be incidental magnetization transfer (MT) effects from off-resonance 180° or similar pulses used during FSE acquisitions. Using two pool modelling, MT decreases the observed mobile proton density ρ_{MOBS} in the free pool and decreases the observed T1 ($T1_{OBS}$) of the free pool in proportion to the reduction in ρ_{MOBS}. This reduction may be quite substantial and decrease normal ρ_{MOBS} and $T1_{OBS}$ by as much as 50%. In general, in disease MT effects are decreased so the reduction in ρ_{MOBS} and $T1_{OBS}$ in diseased tissue due to MT is generally less than that in normal tissue. This is manifested as an apparent increase in ρ_{MOBS} and $T1_{OBS}$ in diseased tissue relative to normal tissue. This is in addition to any increases in T1 in diseased tissue for other reasons, e.g., pathological change such as edema.

2D FSE images with higher echo train lengths (ETLs) utilize more 180° pulses and thus produce a corresponding increase in MT effects during multislice acquisitions. These produce a greater reduction in values of $T1_{OBS}$ and so need shorter nulling TIs. MT effects are less with gradient echo acquisitions as usually used with 3D acquisitions. As a result, $T1_{OBS}$ may be longer with 3D gradient echo acquisitions than with 2D FSE acquisitions and so their nulling TIs may need to be correspondingly longer. The contrast between normal and abnormal tissues may also be lower with gradient echo acquisitions.

In summary, when we employ a workhorse 2D multislice sequence inversion recovery FSE, which uses numerous off resonance RF pulses with high flip angles, this drives down ρ_{MOBS} and $T1_{OBS}$ more in normal tissues than abnormal tissues. The result is an increase in the observed T1 of abnormal tissue relative to normal tissue and this is synergistic with increases in T1 in abnormal tissue for other reasons.

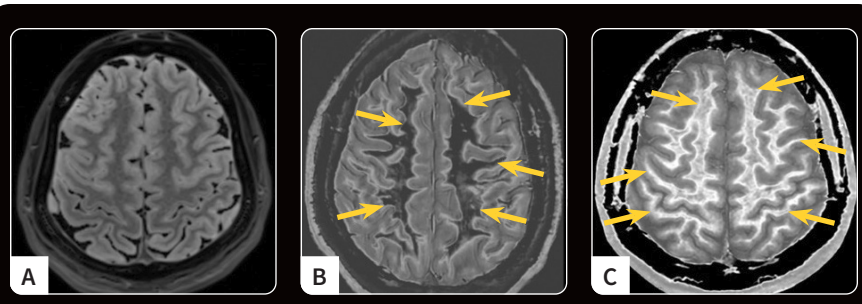

Figure 6. (A and C) Positionally matched images of the brain in a 24-year-old male patient with mTBI and (B) a normal control. (A) T2 FLAIR image in the patient which shows no abnormality. (B) A narrow mD dSIR image of the brain in the normal control. The white matter in the central region of this image has a normal low signal (dark) appearance (arrows). (C) A narrow mD dSIR image performed in the patient with the same sequence as in the control. This image shows all the patient's white matter with abnormal high signal (light, arrows) rather than the normal low signal (dark) appearance in (B) the control (arrows). There is a night and day difference in signal between (B) normal and (C) abnormal white matter. (B) High signal boundaries are seen between normal white matter and normal gray matter that are less obvious in (C) because of the high signal in the abnormal white matter.

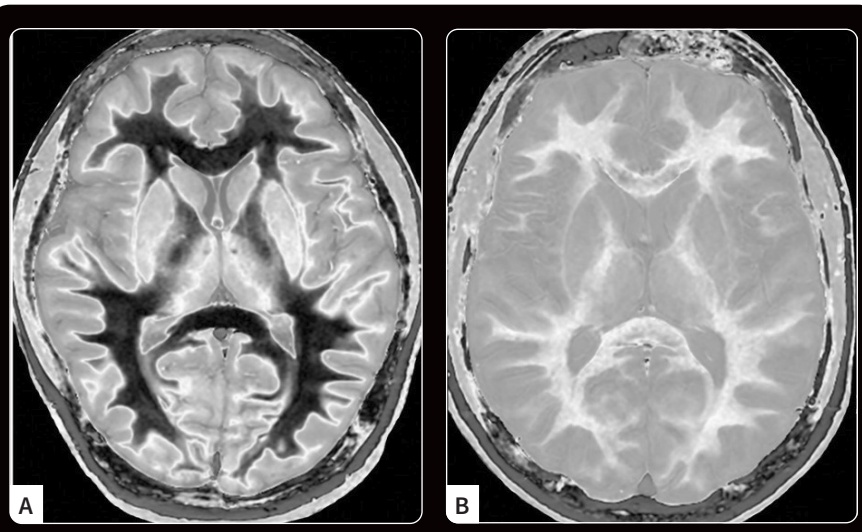

Figure 7. (A) Normal control and (B) patient with mTBI showing a whiteout sign and grayout signs (narrow mD dSIR images). The normal control shows the heads of the caudate nuclei with higher signal than the adjacent CSF. Contrast is also seen between the cortex and CSF. (B) The patient shows a whiteout sign. There are grayout signs in the thalami and putamina. In addition, contrast between the heads of the caudate nuclei and CSF is lost and there is little or no contrast between cortex and CSF, which are isointense. These are additional grayout signs. No abnormality was seen on the T2 FLAIR images in the normal control or patient.

Implementation

The implementation and development of UHC MR began on Mātai's SIGNA™ Premier 3.0T MR system in 2022 with a divided subtracted inversion recovery, or dSIR, sequence that was 10 times more sensitive

to white matter changes than conventional inversion recovery sequences. In several patients with multiple sclerosis (MS), plaques were much better seen than with the traditional T2 FLAIR sequence.

The sequence is only sensitive to changes in T1 within a well-defined interval (of T1), so Mātai also investigated whether a wider Domain of T1 values could be captured and used to create more targeted narrow mD images.

Efforts to optimize the sequence as a 3D acquisition have been successful. With UHC MR 3D acquisitions, the full extent of disease can be seen, including the precise position of lesions within the spinal cord.

Mild traumatic brain injury (mTBI)[7]

The Mātai group has examined a cohort of 30 symptomatic patients with a history of TBI. When compared with normal volunteers, the patients with prior TBIs have widespread high signal in their brain white matter or whiteout sign, showing that there has been a generalized increase in T1 throughout white matter. In a case control study, only the TBI patients showed these changes when compared to a normal cohort.

In a patient with a very mild head injury, a whiteout sign was visualized at 18 hours post injury and then showed a complete reversal back to normal at 64 hours post injury.

A scoring system was developed for the whiteout sign and independently reviewed by two radiologists. They had 98% agreement and the K values were above 0.9.

Conventional MR usually shows no change in mTBI, but narrow mD dSIR imaging frequently shows extensive high signal areas in white matter (the whiteout sign) as seen in Figure 6. The sign is generally attributed to neuroinflammation, however, edema, demyelination and degeneration may also have a role.

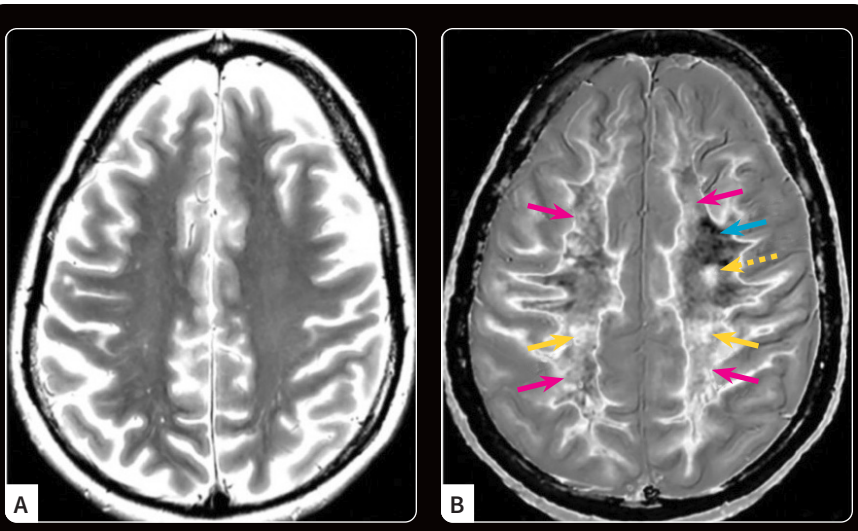

Figure 8. A 41-year-old female patient with MS in remission. (A) 2D T2-FSE and (B) narrow mD dSIR images at the same level. (A) No abnormality is seen. (B) A focal lesion is seen (yellow dashed arrow) and the corticospinal tracts show a high signal (yellow arrows). In addition, there is patchy increased signal in white matter (pink arrows) with only a small region showing a normal or near normal low signal appearance (blue arrow) compared with the extensive normal black areas in white matter shown in Figure 6B. (B) High contrast and high spatial resolution contrast are seen at the boundaries between normal white matter and normal gray matter. These features are less obvious in areas where the white matter has abnormal high signal.

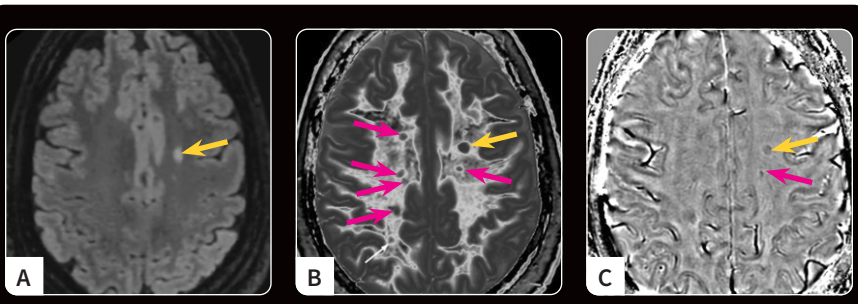

Figure 9. A 32-year-old female with MS during a relapse. (A) T2 FLAIR, (B) synthetically generated narrow mD dSIR and (C) filtered gradient echo images. (A) On the T2 FLAIR image, one lesion is seen (yellow arrow). The surrounding white matter appears normal. (B) On the dSIR image, the lesion shown on the T2 FLAIR image is seen (yellow arrow) as well as other lesions (pink arrows). High signal boundaries around lesions are also seen. (C) Some of these lesions show paramagnetic rims on the filtered gradient echo image (arrows). In addition, (B) most of the white matter is high signal corresponding to a high grade 4/5 whiteout sign.[1] The whiteout sign is not seen on the (A) T2 FLAIR image.

There are also grayout signs. Figure 7A shows a normal control with obvious contrast between the heads of the caudate nuclei and the adjacent CSF, as well as between the cortex and CSF. Figure 7B shows a patient with mTBI who has a whiteout sign. There is a loss of contrast in the thalamus and putamen. In addition, contrast is lost between the heads of the caudate nuclei and CSF, as well as between cortex and CSF, which appear isointense. These are grayout signs. Thus, the patient has a combination of whiteout and grayout signs.

Multiple sclerosis (MS)[8]

Patients with MS develop focal areas of demyelination or plaques that are seen with MR imaging using T2-weighted sequences such as T2 FLAIR and T2-weighted fast spin echo (T2 FSE) in the white matter of the brain.

Several MS patients presented acutely with relapses. They showed focal plaques on their MR images. In addition, there were generalized white matter changes throughout the brain consistent with whiteout signs. An MS patient, who was scanned prior to having an exacerbation

of her symptoms and again during a relapse, provided further validation of the association between symptoms and generalized white matter changes visualized with dSIR.

There are a significant number of MS patients – some population studies suggest a quarter or more – who have relapses of their symptoms, but their conventional MR is unchanged.[9] This creates a dilemma in treating these patients. For the first time, we now see whiteout signs with extensive abnormalities in all of their white matter in patients with relapses. This remits with recovery. The whiteout sign is likely to be a valuable marker of disease exacerbation.

Across the board in MS, changes on dSIR images have been visualized in areas of the brain that appeared normal on standard T2 FLAIR or T2-FSE sequences. While the exact histological basis for these changes has not yet been established, MS is regarded as a neuroinflammatory disease and neuroinflammation is likely to have a central role in the pathogenesis of these changes.

Focal lesions, as well as patchy white matter changes, may be seen in areas that appear normal on T2-FSE images in a patient in remission (Figure 8). In a case during a relapse, one lesion is seen on the T2 FLAIR image in Figure 9A (yellow arrow). This lesion is also seen in Figure 9B on the dSIR image (yellow arrow). There are an additional six lesions (pink arrows) in Figure 9B. Some MS lesions in Figure 9B have high signal boundaries. Some of these lesions have paramagnetic rims on filtered susceptibility weighted images (arrows, Figure 9C). In addition, there are widespread abnormal areas in white matter, which are only seen on the dSIR images (Figure 9B). These changes are typically bilateral, symmetrical and have a generally uniform increase in signal consistent with a whiteout sign. To date, whiteout signs have only been seen in MS patients during a relapse.

In four MS patients, the spinal cord showed obvious changes that were barely visible or not seen with conventional imaging (Figure 10).

In patients with optical neuritis, widespread changes can be detected along the optic nerve with dSIR sequences. These are not visualized with conventional sequences.

Other diseases

There are other diseases such as hypoxic-ischemic injury to the brain[10] and cerebral tumors[11] where whiteout signs are seen.

In a case of untreated rectal cancer metastasis, the T2 FLAIR image (Figure 11A) shows the tumor (arrow) and surrounding edema clearly. In Figure 11B, which is a matched synthetically generated narrow mD dSIR image, extensive bilateral symmetrical high signal white matter abnormalities are seen outside of the tumor and edema in the left hemisphere as well as in the right hemisphere in regions where no abnormality is seen on the T2 FLAIR image. There is sparing of the anterior and posterior central corpus callosum and the peripheral white matter consistent with a florid whiteout sign (grade 5 out of 5) (Figure 11B).

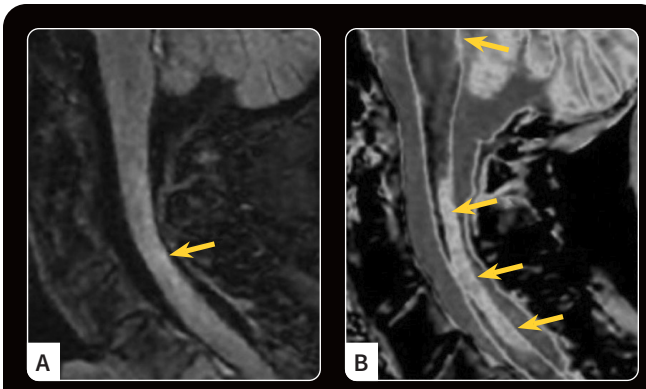

Figure 10. A 43-year-old female patient with MS. (A) Sagittal 3D T2 FLAIR and (B) 3D wide mD dSIR images. (A) The T2 FLAIR image shows a poorly defined area of increased signal in the cervical cord (arrow). (B) The dSIR image shows a high contrast lesion with sharply defined ("punched out") boundaries in the cervical cord (lower three arrows). This is much more extensive than in (A). (B) An additional lesion is seen in the medulla on the dSIR image (highest arrow) but not on the (A) T2 FLAIR image.

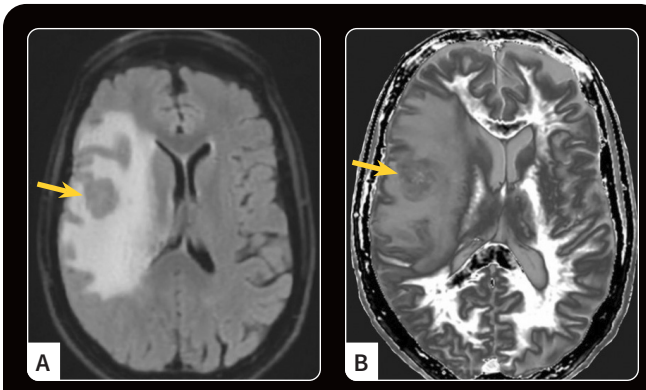

Figure 11. A 76-year-old male patient with an untreated rectal cancer metastasis to the brain. (A) T2 FLAIR and (B) similarly located synthetic narrow mD dSIR T1-BLAIR (BipoLAr fIlteR) images. The metastasis has an intermediate signal on the (A) T2 FLAIR image (arrow) and is surrounded by high signal edema. No abnormality is seen in the left hemisphere apart from small periventricular change at the anterior horn of the lateral ventricle. (B) The dSIR image shows the metastasis as intermediate signal (arrow) and the surrounding edema as mid gray signal. On the dSIR image the white matter in both the right and left hemispheres shows bilateral symmetrical very high signal apart from the anterior and posterior central corpus callosum and the peripheral white matter. This is a maximum grade whiteout sign (i.e., grade 5 out of 5). (A) No abnormality is seen on the T2 FLAIR image in the areas that show the (B) very high signal on the dSIR image. Features due to larger changes in T2 are seen on the T2 FLAIR images and those due to smaller changes in T1 are seen on the T1-BLAIR image.

Technical and clinical validation

Technical validation of the dSIR sequence has been performed in phantoms and human volunteers.[12,13] The measured values of T1 correspond with known values of T1 in phantom fluids and measurements of T1 with conventional techniques in volunteers. In addition, the pattern of change of signal with T1 conformed to the theoretical predictions shown in Figure 5C in both studies.[12,13] Validation of the sequence in larger populations is the next step in research, including qualitative validation, as well as measurement of T1 values and clinical correlations.

Clinical implications

There are many diseases or injuries in the brain, such as mTBI, where typical state-of-the-art imaging is normal, yet dSIR sequences show changes to the brain.[14]

One of our mTBI patients is a neuropsychiatrist (Dr. Gil Newburn), who previously had a brain MR at Mātai. He fell and sustained a mTBI. He was scanned again and showed a whiteout sign and grayout signs. Dr. Newburn was also able to record his symptoms and correlate them with the imaging findings in detail.

Conclusion

One of the outstanding advantages of UHC MR is that it can be implemented on virtually any scanner. It does not require an increase in field strength to 9.4T or 11.7T to obtain an order of magnitude increase in contrast. A major advance in clinical performance can be obtained on existing scanners at very little cost.

Developments are continuing rapidly with new forms of mathematics, such as log subtracted inversion recovery[15] sequences and new approaches to MR physics, such as synergistic contrast diffusion.

References

1. Young IR, Szeverenyi NM, Du J, Bydder GM. Pulse sequences as tissue property filters (TP-filters): a way of understanding the signal, contrast and weighting of magnetic resonance images. Quant Imaging Med Surg 2020;10:1080-120.
2. Ma YJ, Shao H, Fan S, et al. New options for increasing the sensitivity, specificity and scope of synergistic contrast magnetic resonance imaging (scMRI) using Multiplied, Added, Subtracted and/or FiTted (MASTIR) pulse sequences. Quant Imaging Med Surg 2020;10:2030-65.
3. Ma YJ, Moazamian D, Cornfeld DM, et al. Improving the understanding and performance of clinical MRI using tissue property filters and the central contrast theorem, MASDIR pulse sequences and synergistic contrast MRI. Quant Imaging Med Surg. 2022;12(9):4658-4690.
4. Ma Y-J, Moazamian D, Port JD, et al. Targeted magnetic resonance imaging (tMRI) of small changes in the T1 and spatial properties of normal and near normal appearing white and gray matter in disease of the brain using divided subtracted inversion recovery (dSIR) and divided reverse subtracted inversion recovery (drSIR) sequences. Quant Imaging Med Surg 2023;13(10):7304-7337.
5. Cornfeld D, Condron P, Newburn G, et al. Ultra-High Contrast MRI: Using Divided Subtracted Inversion Recovery (dSIR) and Divided Echo Subtraction (dES) Sequences to Study the Brain and Musculoskeletal System. Bioengineering (Basel). 2024;11(5):441.
6. Bydder M, et al. Investigating the unintended influence of magnetization transfer effects on tissue contrast and signal suppression in UHC MRI sequences. ISMRM May 2025 Annual Meeting, Hawaii (in press).
7. Newburn G, McGeown JP, Kwon EE, et al. Targeted MRI (tMRI) of small increases in the T1 of normal appearing white matter in mild traumatic brain injury (mTBI) using a divided subtracted inversion recovery (dSIR) sequence. OBM Neurobiology 2023;7(4):1-27.
8. Condron P, Cornfeld DM, Bydder M, et al. Ultra-high contrast (UHC) MRI of the brain, spinal cord and optic nerves in multiple sclerosis using directly acquired and synthetic bipolar filter (BLAIR) images. Diagnostics 2025;15(3):329.
9. Gavoille A, Rollof F, Casey R, et al. Acute clinical events identified as relapses with stable magnetic resonance imaging in multiple sclerosis. JAMA Neurol 1024;81:814-823.
10. Newburn G, Condron P, Kwon EE, et al. Diagnosis of delayed post-hypoxic leukoencephalopathy (Grinker's myelinopathy) with MRI using divided subtracted inversion recovery (dSIR) sequences: time for reappraisal of the syndrome? Diagnostics 2024;14(4):418.
11. Condron P, et al. Ultra-high contrast (UHC MRI) of white matter surrounding cerebral tumors using divided subtracted inversion recovery sequences. ISMRM May 2025 Annual Meeting, Hawaii (in press).
12. Bydder M, Condron P, Cornfeld DM, et al. Validation of an ultra-high contrast divided subtracted inversion recovery technique using a standard T1 phantom. NMR Biomed 2024;e5269.
13. Losa L, Peruzzo D, Galbiati S, Locatelli F, Agarwal N. Enhancing T1 signal of normal-appearing white matter with divided subtracted inversion recovery: a pilot study in mild traumatic brain injury. NMR Biomed 2024;37(10):e5175.
14. Condron P, Cornfeld DM, Scadeng M, et al. Ultra-high contrast MRI: the whiteout sign shown with divided subtracted inversion recovery (dSIR) sequences in post-insult leukoencephalopathy syndromes (PILS). Tomography 2024;10(7):983-1013.
15. Bydder M, Cornfeld DM, Melzer TR et al. Log subtracted inversion recovery. Magn Reson Imaging 2025;117:110328.